Transient electron dynamics in a vibrating quantum dot in the Kondo regime

IOP Publishing Journal of Physics: Condensed Matter

J. Phys.: Condens. Matter **23** (2011) 125302 (7pp) doi:10.1088/0953-8984/23/12/125302

Transient electron dynamics in a vibrating quantum dot in the Kondo regime

A Goker

Department of Physics, Bilecik University, Gulumbe, 11210, Bilecik, Turkey

Received 6 December 2010, in final form 20 January 2011
Published 9 March 2011
Online at stacks.iop.org/JPhysCM/23/125302

Abstract

We employ the time-dependent non-crossing approximation to investigate the joint effect of strong electron–electron and electron–phonon interaction on the instantaneous conductance of a single-molecule transistor which is abruptly moved into the Kondo regime by means of a gate voltage. We find that the instantaneous conductance exhibits decaying sinusoidal oscillations on the long timescale for infinitesimal bias. The ambient temperature and electron–phonon coupling strength influence the amplitude of these oscillations. The frequency of the oscillations is found to be equal to the phonon frequency. We argue that the origin of these oscillations can be attributed to the interference between the emerging Kondo resonance and its phonon sidebands. We discuss the effect of finite bias on these oscillations.

(Some figures in this article are in colour only in the electronic version)

1. Introduction

Molecular transport junctions that consist of a molecule inserted between contacts have long fascinated both physicists and chemists, since it was proposed more than three decades ago that they could be used one day as building blocks for future electronic devices. The emergence of the field of molecular electronics originates from this suggestion [1]. The nanotechnology revolution which took place in the mid-1980s paved the way to precise control of nanostructures and enabled us to perform experiments that were beyond anyone's realm previously [2]. Experimental confirmation of the Kondo effect, which was predicted two decades ago theoretically [3, 4], first for quantum dots [5–7] and then for single-molecule transistors [8, 9], opened an avenue to the possible merging of the fields of spintronics and molecular electronics [10]. The goal of the field of molecular spintronics is to investigate spin-dependent transport in molecular electronic devices [11]. Therefore, the Kondo effect acts as a supplemental spin-dependent mechanism that might strongly affect the spin transport in quantum dots.

In his groundbreaking work [12], Kondo discovered that the resistivities of bulk metals which contain magnetic impurities with localized unpaired spins would be enhanced at low temperatures. This enhancement was dubbed the Kondo effect later on. The underlying microscopic mechanism for the Kondo effect has been identified as the formation of a spin singlet resulting from the interaction of the unpaired localized electron and continuum electrons near the Fermi level in the metal [13].

Quantum dots are artificial atoms that can contain an integer number of electrons [14]. It is important to confine an odd number of electrons in a quantum dot to study the Kondo effect. This gives rise to a net spin in the dot just like in a bulk metal. However, coupling of this net spin to the fermionic bath in the metallic leads opens a new transport channel in the quantum dot and the conductance is enhanced at low temperatures instead of the resistivity in bulk metals. A sharp many-body resonance at the dot density of states pinned to the Fermi level of the contacts is responsible for the enhancement. This conductance enhancement is a robust way of obtaining current flow in odd number Coulomb blockade valleys and thus preventing current inhibition in single-electron devices.

Sudden shifting of the gate or source–drain voltage has been studied in detail previously [15–18] and three unique timescales have been clearly identified in the ensuing transient current [19–22]. The non-Kondo timescale is associated with the initial fast rise of the current accompanied by reshaping of the Breit–Wigner resonance. On the other hand, formation of the Kondo resonance and its reaching a broad quasi-smooth structure with a linewidth of the order of Kondo temperature is the hallmark of the longer Kondo timescale. Splitting of the Kondo resonance for finite bias corresponds to the third and longest timescale. This timescale can be determined by measuring the decay rate of the split Kondo peak

oscillations [19]. Later studies focused on the asymmetric coupling of the dot to the contacts and concluded that an interference between the Kondo resonance and the van Hove singularities in the density of states of the leads may give rise to sinusoidal oscillations in the transient current [23, 24]. Recent extension of the diagrammatic Monte Carlo method [25] to nonequilibrium impurity problems [26] confirmed the sensitive dependence of the transient current on the bandwidth of the contacts [27].

The history of electron–phonon interaction in molecular transport junctions is quite long, as has been summarized in a recent review [28]. Phonon assisted electron transport in molecular transport junctions can be broadly classified on the basis of the relative timescales and energy scales in the process. The strength of the electron–phonon interaction is judged relative to the molecule–electrode coupling. In this respect, weak and strong electron–phonon coupling regimes emerge.

The former regime, namely the weak electron–phonon interaction, corresponds to the nonresonant phonon assisted electron tunneling encountered in inelastic electron transport spectroscopy [29, 30]. The development of scanning tunneling microscopy and spectroscopy proved to yield invaluable tools for inelastic electron transport spectroscopy, for defining and characterizing the conductance properties of molecular species. It is justified to use Migdal–Eliashberg theory [31, 32] in this regime. As a result, the second-order perturbation theory for the electron–phonon coupling over the Keldysh contour leads to the Born approximation. Various versions of the self-consistent Born approximation has been used in several theoretical studies [33–36].

The latter strong coupling regime corresponds to resonant tunneling which involves a longer electron lifetime and stronger electron–phonon interaction. Perturbation theory fails in this regime and a polaron is formed in the junction. Signatures of the resonant tunneling are manifested as sidebands of the main Kondo resonance in differential conductance [37]. There are several studies investigating this case in the steady state. Preliminary accounts of the electron–phonon coupling computed the dot Green's function using the equation of motion method [38] and treating the contacts as unaffected by the bosons in the wide band limit [39]. Both approaches concluded that the electron–phonon interaction results in sidebands only on one side of the main elastic peak in the density of states. In later studies, it has been suggested that this is due to an invalid approximation being employed in calculating the retarded Green's function and that the phonon sidebands should appear on both sides of the elastic peak [40–42]. Perturbative renormalization group calculations confirmed this latter conclusion [43].

In the strong electron–phonon coupling regime, the approach invoking the Lang–Firsov canonical transformation and non-crossing approximation also found sidebands on both sides of the main Kondo resonance in the time averaged ac conductance; however this last method concluded that the zero-bias Kondo resonance has been greatly suppressed [44]. Recently, investigation of the electron–phonon interaction in the Kondo regime using the nonequilibrium equation of motion method has found that increasing the electron–phonon interaction strength gradually destroys the Kondo effect [45]. This has been attributed to the destruction of the coherence in the system by the electron–phonon interaction and the shift of the energy level due to rearrangement of the phonons.

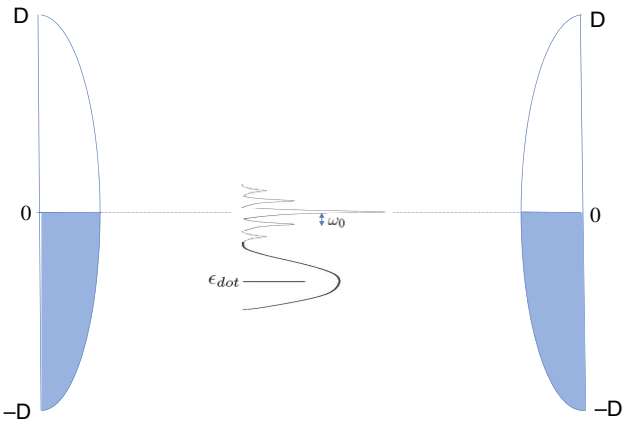

Figure 1. This figure depicts the density of states of the left and right contacts along with the density of states of the quantum dot in the final state, schematically.

In this paper, we will investigate a scenario in which a Coulomb blockaded molecular quantum dot is suddenly shifted from a position well below the Fermi level of the leads to a position where the Kondo effect is present by means of a gate voltage. Previous studies unambiguously demonstrated that the strong electron–electron interactions give rise to a Kondo resonance pinned to the Fermi level of the contacts decorated with sidebands on each side due to the electron–phonon coupling. However, little is known about the real-time electron dynamics of this system as a response to abrupt perturbations except the findings of a recent study using the mean-field approximation for a spinless model [46]. The setup of the system under consideration is shown schematically in figure 1. The goal of this paper is to fill this gap by reporting the instantaneous conductance after an interacting vibronic dot's energy level has been moved to its final position.

2. Theory

We model this device by a single spin degenerate level of energy $\epsilon_{\rm dot}$ attached to leads through tunnel barriers and coupled to a single phonon mode. This model is referred to as the Holstein Hamiltonian. In this paper, we will be concerned with the strong electron–phonon coupling regime where the electron–phonon term can be discarded with a canonical transformation. We carry out the auxiliary boson transformation for the resulting Hamiltonian where the ordinary electron operator on the dot is rewritten in terms of a massless boson operator and a pseudofermion operator. The $U \rightarrow \infty$ limit is obtained by imposing the condition that the sum of the number of bosons and the pseudofermions is equal to unity.

The aforementioned Hamiltonian has three pieces describing the contacts, the quantum dot and the process of tunneling

between them and it can be written as

$$H(t) = H_{\rm C} + H_{\rm D}(t) + H_{\rm T}(t) \tag{1}$$

where

$$\begin{aligned} H_{\rm C} &= \sum_{k\alpha\sigma} (\epsilon_{k\alpha} - \mu_\alpha) c^\dagger_{k\alpha\sigma} c_{k\alpha\sigma} \\ H_{\rm D}(t) &= \sum_\sigma [\epsilon_{\rm dot}(t) + \lambda(a + a^\dagger)] d^\dagger_\sigma d_\sigma + U d^\dagger_\uparrow d_\uparrow d^\dagger_\downarrow d_\downarrow \\ &\quad + \omega_0 a^\dagger a \\ H_{\rm T}(t) &= \sum_{k\alpha\sigma} (V_{k\alpha}(t) c^\dagger_{k\alpha\sigma} d_\sigma + \text{h.c.}). \end{aligned} \tag{2}$$

In this Hamiltonian, $d^\dagger_\sigma (d_\sigma)$ and $c^\dagger_{k\alpha\sigma} (c_{k\alpha\sigma})$ with $\alpha = {\rm L}, {\rm R}$ create (annihilate) an electron of spin σ in the quantum dot in the left (L) and right (R) leads, respectively. $V_{k\alpha}$ and μ_α are the tunneling amplitudes and chemical potentials for the left and the right leads. $a^\dagger$ (a) creates (annihilates) a phonon within the quantum dot. λ is the strength of the electron–phonon coupling and ω_0 is the phonon frequency. We will deal with a single phonon mode in the Hamiltonian and ignore its coupling to a thermal environment which would appear as a secondary phonon mode. This assumption is justified as long as the whole system can be kept at the same temperature T. We will use atomic units with $\hbar = k_{\rm B} = e = 1$ during the rest of this paper.

We will take the hopping matrix elements to be equal with no explicit time and energy dependence. Under this assumption, broadening of the dot level can be parameterized as $\Gamma(\epsilon) = \bar{\Gamma}\rho(\epsilon)$ where $\bar{\Gamma}$ is a constant given by $\bar{\Gamma} = 2\pi |V(\epsilon_{\rm f})|^2$ and $\rho(\epsilon)$ is the density of states function of the contacts. We will use parabolic densities of states in both contacts with the same bandwidth.

If the electron–phonon coupling is weak, the electron–phonon coupling term can be treated perturbatively. In this paper, we will be concerned with the opposite case, where the electron–phonon coupling is sufficiently strong compared to the tunnel couplings. In this regime, the perturbative solution fails and a suitable canonical transformation must be applied to eliminate the electron–phonon coupling term. The most versatile choice is the unitary Lang–Firsov canonical transformation [47] given by

$$S = \exp\left[\frac{\lambda}{\omega_0} \sum_\alpha d^\dagger_\sigma d_\sigma (a^\dagger - a)\right]. \tag{3}$$

This transformation gives

$$S a S^\dagger = a - \frac{\lambda}{\omega_0} \sum_\sigma d^\dagger_\sigma d_\sigma \qquad S d_\sigma S^\dagger = d_\sigma X \tag{4}$$

where the operator X is given by

$$X = \exp\left[-\frac{\lambda}{\omega_0}(a^\dagger - a)\right]. \tag{5}$$

The electron operators d_σ $(d^\dagger_\sigma)$ in $H_{\rm T}(t)$ are multiplied by X $(X^\dagger)$ as a result of this transformation, indicating that the tunneling electrons create and destroy a phonon cloud. This leads to polaron formation at the junction.

Under this canonical transformation, the dot Hamiltonian turns into

$$\begin{aligned} \bar{H}_{\rm D}(t) = S H_{\rm D}(t) S^\dagger &= \sum_\sigma \left(\epsilon_{\rm dot}(t) - \frac{\lambda^2}{\omega_0}\right) d^\dagger_\sigma d_\sigma \\ &\quad + \left(U - \frac{2\lambda^2}{\omega_0}\right) d^\dagger_\uparrow d_\uparrow d^\dagger_\downarrow d_\downarrow + \omega_0 a^\dagger a. \end{aligned} \tag{6}$$

It is clear from this result that the dot level and the Hubbard interaction strengths are renormalized as $\bar{\epsilon}_{\rm dot}(t) = \epsilon_{\rm dot}(t) - (\lambda^2/\omega_0)$ and $\bar{U} = U - (2\lambda^2/\omega_0)$, respectively, as a result of this transformation.

In the strong electron–phonon coupling regime, i.e. when a polaron is formed at the junction, mean-field theory can be applied and the expectation value of the operator X given by

$$\langle X \rangle = \exp\left[-\frac{\lambda^2}{\omega_0^2}\left(N_{\rm ph} + \frac{1}{2}\right)\right] \tag{7}$$

can serve as a substitute for the operator.

Even though U has been renormalized to $\bar{U} = U - (2\lambda^2/\omega_0)$, it is still positive and it overwhelms the linewidth Γ for realistic systems. Hence, typically one takes $\bar{U} \to \infty$. This forbids double occupancy of the dot level. The downside of this advantage is that the standard diagrammatic techniques are no longer applicable. This problem can be circumvented by introducing a massless boson operator and a pseudofermion operator on the molecule. The original electron operators can be written in terms of these operators as

$$d_\sigma(t) = b^\dagger(t) f_\sigma(t) \qquad d^\dagger_\sigma(t) = f^\dagger_\sigma(t) b(t) \tag{8}$$

subject to the requirement

$$Q = b^\dagger b + \sum_\sigma f^\dagger_\sigma f_\sigma = 1 \tag{9}$$

which ensures single occupancy of the dot level. The resulting slave boson Hamiltonian becomes

$$\begin{aligned} \bar{H}(t) &= \sum_{k\alpha\sigma} (\epsilon_{k\alpha} - \mu_\alpha) c^\dagger_{k\alpha\sigma} c_{k\alpha\sigma} + \sum_\sigma \bar{\epsilon}_{\rm dot} f^\dagger_\sigma f_\sigma + \omega_0 a^\dagger a \\ &\quad + \sum_{k\alpha\sigma} (\tilde{V}_{k\alpha}(t) c^\dagger_{k\alpha\sigma} f_\sigma b^\dagger + \text{h.c.}) \end{aligned} \tag{10}$$

where the tunnel coupling and dot level are renormalized as $\tilde{V}_{k\alpha}(t) = V_{k\alpha}(t)\langle X \rangle$ and $\bar{\epsilon}_{\rm dot}(t) = \epsilon_{\rm dot}(t) - (\lambda^2/\omega_0)$, respectively. λ^2/ω_0 is called the classical energy of distortion or reorganization energy which quantifies the polaron formation compared to the phonon frequency ω_0. These constitute the energy scales in this problem along with $\bar{\Gamma}$, which corresponds to the tunneling rate.

We then invoke the well established non-crossing approximation (NCA) to determine the pseudofermion and slave boson self-energies. The NCA has been shown to give accurate results for dynamical quantities save for temperatures below $T/T_{\rm K} \approx 0.1$ or finite magnetic fields. These two problematic cases will not be dwelt on in this paper.

The net current flowing through the device can be calculated from the resulting Green's functions. We will

write the net current as $I(t) = I_{\rm L}(t) - I_{\rm R}(t)$, where $I_{\rm L}(t)(I_{\rm R}(t))$ represents the net current from the left (right) contact through the left (right) barrier to the quantum dot. The most general expression for the net current [48] has previously been derived by using pseudofermion and slave boson Green's functions [23]. Here, we will adapt it to the present situation. For symmetric coupling, the net current is reduced to

$$I(t) = -2\bar{\Gamma}\,\mathrm{Im}\left(\int_{-\infty}^{t} \mathrm{d}t_1\, G^{\rm R}(t,t_1)(f_{\rm L}(t-t_1) - f_{\rm R}(t-t_1))\right) \tag{11}$$

and the retarded Green function can be expressed as

$$G^{\rm R}(t,t_1) = -\mathrm{i}\theta(t-t_1)[\langle d_\sigma(t) d_\sigma^\dagger(t_1)\rangle\langle X(t)X^\dagger(t_1)\rangle + \langle d_\sigma^\dagger(t_1) d_\sigma(t)\rangle\langle X^\dagger(t_1)X(t)\rangle]. \tag{12}$$

It turns out that the correlators of the operators $X(t)$ and $X^\dagger(t_1)$ can be evaluated exactly. They are given by $\langle X(t)X^\dagger(t_1)\rangle = \mathrm{e}^{\phi(t_1-t)}$ and $\langle X^\dagger(t_1)X(t)\rangle = \mathrm{e}^{\phi(t-t_1)}$. In these expressions, the phase factor is given by

$$\phi(t_1-t) = -g[N_{\rm ph}(1-\mathrm{e}^{-\mathrm{i}\omega_0(t_1-t)}) + (N_{\rm ph}+1)(1-\mathrm{e}^{\mathrm{i}\omega_0(t_1-t)})] \tag{13}$$

where g is defined as $g = \frac{\lambda^2}{\omega_0^2}$ and $N_{\rm ph}$, given by Bose–Einstein distribution $N_{\rm ph} = \frac{1}{\mathrm{e}^{\frac{\hbar\omega_0}{k_{\rm B}T}}-1}$ function, represents the average number of phonons for temperature T and phonon frequency ω_0. It has been pointed out before that the correlators are approximately equal only at sufficiently high temperatures such that $N_{\rm ph}$ is much larger than unity. At low temperatures, taking them equal may produce erroneous results such as producing phonon sidebands only on one side of the main Kondo peak. Therefore, in this paper we will not resort to such an approximation and keep the correlators in separate terms.

The retarded Green's function can then be written as

$$\begin{aligned} G^{\rm R}(t,t_1) &= -\mathrm{i}\theta(t-t_1) \\ &\quad\times [\langle d_\sigma(t) d_\sigma^\dagger(t_1)\rangle \mathrm{e}^{\phi(t_1-t)} + \langle d_\sigma^\dagger(t_1) d_\sigma(t)\rangle \mathrm{e}^{\phi(t-t_1)}] \\ &= -\mathrm{i}\theta(t-t_1)[G^{>}_{\rm real}(t,t_1)\mathrm{e}^{\phi(t_1-t)} + G^{<}_{\rm real}(t,t_1)\mathrm{e}^{\phi(t-t_1)}]. \end{aligned} \tag{14}$$

Using the slave boson and pseudofermion decomposition of the original fermion operators on the molecule, the retarded Green's function can be recast as

$$G^{\rm R}(t,t_1) = -\mathrm{i}\theta(t-t_1)[G^{\rm R}_{\rm pseudo}(t,t_1)B^{<}(t_1,t)\mathrm{e}^{\phi(t_1-t)} + G^{<}_{\rm pseudo}(t,t_1)B^{\rm R}(t_1,t)\mathrm{e}^{\phi(t-t_1)}]. \tag{15}$$

The real-time coupled integro-differential Dyson equations for the retarded and lesser Green's functions are computed in a Cartesian two-dimensional grid. The values are stored in a matrix and the matrix is propagated diagonally in time. The phase factors are attached to the pseudofermion Green's functions in order to incorporate the phonon effects properly [49]. The instantaneous conductance is obtained by performing an integration over the lowest row of the matrix using the expression

$$\begin{aligned} I(t) = 2\bar{\Gamma}\,\mathrm{Re}\Bigg(&\int_{-\infty}^{t} \mathrm{d}t_1\, (G^{\rm R}_{\rm pseudo}(t,t_1)B^{<}(t_1,t)\mathrm{e}^{\phi(t_1-t)} \\ &+ G^{<}_{\rm pseudo}(t,t_1)B^{\rm R}(t_1,t)\mathrm{e}^{\phi(t-t_1)}) \\ &\times (f_{\rm L}(t-t_1) - f_{\rm R}(t-t_1))\Bigg) \end{aligned} \tag{16}$$

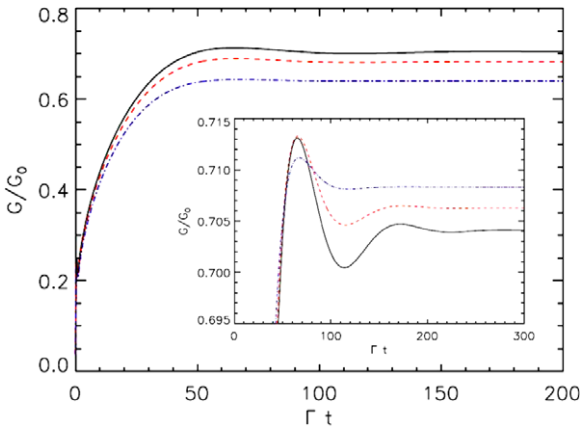

Figure 2. Black (solid), red (dashed) and blue (dash–dotted) curves show instantaneous conductance results as a function of time for $T = 0.0009\Gamma$, $T = 0.0010\Gamma$ and $T = 0.0012\Gamma$, respectively, with $g = 2.25$ after the dot level has been switched to its final position. The inset is the magnified version of the main panel. The curves for high temperatures in the inset have been shifted to enable comparison of the amplitudes.

where $f_{\rm L}(t-t_1)$ and $f_{\rm R}(t-t_1)$ are the convolutions of the density of states functions with the Fermi–Dirac distribution [23]. The conductance G is equal to the current I divided by the bias voltage V. A comprehensive description of our numerical implementation has been published previously [22, 50].

An exquisite many-body state called the Kondo effect arises when the dot level is positioned below the Fermi energy at sufficiently low temperatures. The net spin localized within the dot and the Fermi sea of electrons in the contacts hybridize to form a spin singlet. This results in a sharp resonance fixed to the Fermi levels of the contacts in the dot density of states. The linewidth of the Kondo resonance can be approximated by an energy scale $T_{\rm K}$ (Kondo temperature) given by

$$T_{\rm K} \propto \left(\frac{D\Gamma}{4}\right)^{\frac{1}{2}} \exp\left(-\frac{\pi|\epsilon_{\rm dot}|}{\Gamma}\right) \tag{17}$$

where D is a high energy cutoff equal to the half-bandwidth of the conduction electrons and Γ corresponds to the value of the coupling between the dot and the contacts $\Gamma(\epsilon)$ at $\epsilon = \epsilon_{\rm F}$.

Our aim in this paper is to theoretically investigate a case in which the dot level is displaced from its equilibrium level abruptly by means of a gate voltage. We will be particularly interested in a system which has been studied before in the absence of any electron–phonon coupling. Its dot level is abruptly moved from $\epsilon_{\rm dot} = -5\Gamma$ to $\epsilon_{\rm dot} = -2\Gamma$ at $t = 0$ where $\Gamma = \bar{\Gamma}\rho(\epsilon_{\rm f})$. We will report the instantaneous conductance right after the dot is moved to its final position. In the following discussion, we will take the phonon frequency as $\omega_0 = 0.06\Gamma$.

3. Results

We begin our analysis with the instantaneous conductance results immediately after the dot level has been switched to its final position. The results shown in figure 2 correspond to

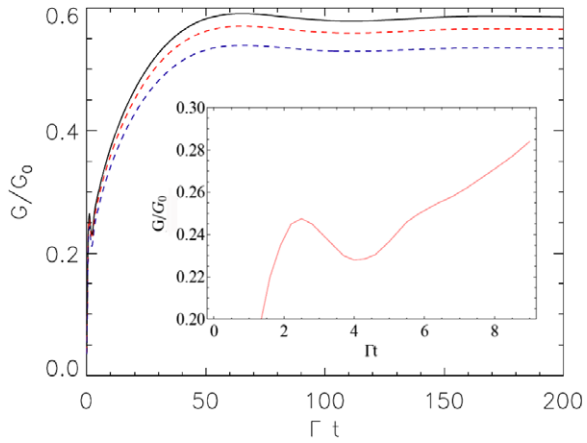

Figure 3. Black (solid), red (dashed) and blue (dash–dotted) curves in the main panel show instantaneous conductance results as a function of time for $T = 0.0009\Gamma$, $T = 0.0010\Gamma$ and $T = 0.0012\Gamma$, respectively, with $g = 3.75$ after the dot level has been switched to its final position. The inset is the magnification of the $T = 0.0010\Gamma$ curve on the short timescale.

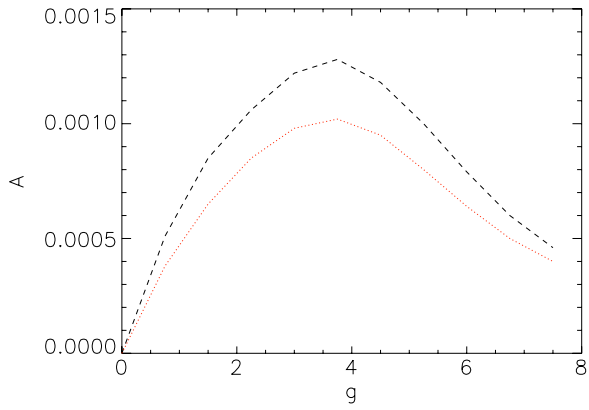

Figure 4. Black (dashed) and red (dotted) curves show the amplitude of the second peak in the conductance oscillation as a function of the electron–phonon coupling strength g for $T = 0.0009\Gamma$ and $T = 0.0010\Gamma$, respectively. The amplitudes have been measured with respect to the steady state (i.e. $\Gamma t \to \infty$) conductance values.

three different temperatures for a constant nonzero electron–phonon coupling g, which corresponds to $\frac{\lambda^2}{\omega_0^2}$. Instantaneous conductance results in the absence of any electron–phonon coupling have been reported previously [19]. The Kondo timescale occurs between the end of the short timescale and the attainment of a plateau by the instantaneous conductance. Kondo resonance starts developing on this timescale. It takes place roughly for $10 < \Gamma t < 60$ in figure 2.

The first key feature that should be mentioned regarding figure 2 is that the steady state conductances (i.e. long time limit) are smaller than in the case without any electron–phonon coupling for all temperatures, as expected [51]. This expectation stems from the fact that the electron–phonon coupling gradually quenches the Kondo effect [45]. This suppression has been explained with a downward shift of the energy level as a result of phonon reorganization. This effect is an obvious consequence of the renormalization of the dot level.

The second and more subtle effect is the sinusoidal oscillation of the current on the Kondo timescale. This effect is difficult to see in the main panel of figure 2; therefore in the inset, we show the magnification of the main panel with shifted conductance curves such that they overlap at the onset of oscillations. In the inset of figure 2, it is clear that the oscillation frequency is the same for all temperatures. Moreover, the amplitude of the oscillations decreases as the ambient temperature increases. It turns out that the oscillation frequency is equal to the phonon frequency ω_0.

In order to test the electron–phonon coupling strength dependence of the oscillation frequency, we increased g and performed the previous calculation at the same temperatures. The result is shown in figure 3. First, the steady state conductance is lower for all temperatures for larger g. This is expected due to the downward level shift as pointed out above. On the other hand, conductance oscillations once more take place with a frequency equal to the phonon frequency ω_0. We should mention that we increased g in figure 3 by increasing λ and keeping ω_0 constant with respect to figure 2 to facilitate a direct comparison. It must be noted that changing the value of ω_0 in our calculations again yields the oscillation frequency of the conductance as ω_0. We checked that the oscillation frequency remains pinned to ω_0 for all g values.

The inset of figure 3 shows the conductance oscillations that take place on the short timescale (i.e. $0 < \Gamma t < 10$). These oscillations are related to the charge transfer and they have been analyzed in detail previously [19, 52]. On this timescale, there are no spin-flip processes associated with the formation of the Kondo resonance. The inset clearly demonstrates that our approach manages to capture these initial oscillations on the short timescale too. A detailed analysis showed that their frequency is proportional to the final dot level (figure 4 in [19]).

We now want to study the amplitude of the oscillations for various electron–phonon coupling strengths and temperatures in a systematic fashion. Figure 4 shows the behavior of the amplitudes as a function of the electron–phonon coupling strength at two different temperatures. The amplitude is zero at $g = 0$ regardless of the temperature, but it starts to increase gradually until it reaches a maximum before $g = 4$. It then starts decreasing and it again approaches zero for large g values. Meanwhile, the amplitude of oscillation is always larger at lower temperature for a given g. We verified that this conclusion holds for other temperatures as well.

It is of great interest to be able to provide a microscopic description for this peculiar behavior of the transient current. One needs to resort to the spectral function of the dot to this end. This can be obtained by taking the Fourier transform of the retarded Green's function. It has been shown before that the phonon sidebands are separated from the main Kondo peak by an integer multiple of the phonon frequency ω_0 [40–43]. We propose that the sinusoidal oscillations seen in the transient current on the Kondo timescale are a result of an interference between the main Kondo peak and its phonon sidebands. For this reason, the frequency of oscillation was found to be equal to ω_0. For a given g parameter, the amplitude of the oscillations increases as the temperature decreases because both the main Kondo peak and its phonon satellites are more developed at lower temperatures, leading to stronger interference.

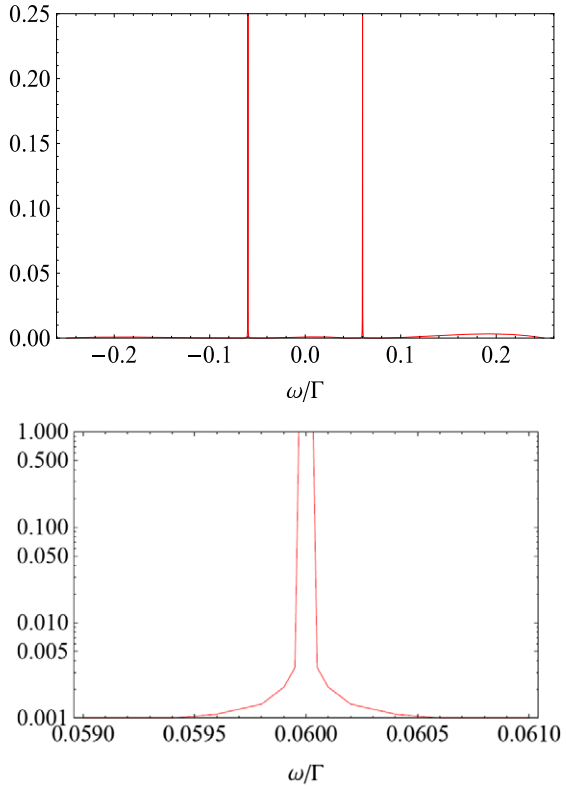

Figure 5. The upper panel shows the Fourier transform of the instantaneous conductance on the long timescale in the infinitesimal bias at $T = 0.0010\Gamma$. The lower panel is a close-up view of the upper panel around the second peak on a logarithmic scale.

On the other hand, sweeping the electron–phonon coupling strength at constant T gives rise to a more complicated situation, as seen in figure 4. Even though the main Kondo peak is developed most fully for $g = 0$ at a given temperature T, resulting in the largest steady state conductance, no oscillation was detected in the infinitesimal bias on the Kondo timescale [19] because the phonon sidebands are completely absent in this case. Consequently, interference is nonexistent and the oscillation amplitude is zero. For small g values, the amplitude of the oscillations gradually increases with g because while the main Kondo peak pinned to the Fermi level becomes inhibited slightly, its phonon sidebands become slightly more pronounced [53]. This naturally leads to stronger interference. However, this behavior changes for moderate values of g. The amplitudes start decreasing around $g = 4$ since destruction sets in for all peaks. Unsurprisingly, the amplitude goes to zero in the large g limit where the Kondo effect disappears completely and none of the peaks survives.

It is important to note that the oscillations take place exclusively with ω_0 in the infinitesimal bias and all the integer multiples of this frequency are completely absent, as one can easily see from the Fourier transform of the instantaneous conductance on the long timescale shown in figure 5. This result is somewhat unexpected since the main Kondo peak should be interfering with other sidebands as well. This issue can be explained easily from an intuitive point of view. As one can see in figure 1 schematically and confirm by taking the

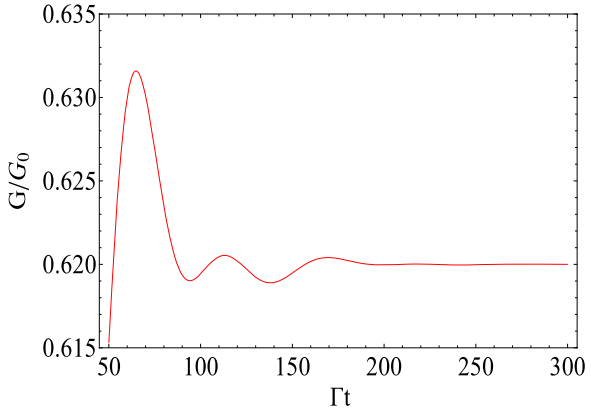

Figure 6. This figure shows the instantaneous conductance as a function of time for $T = 0.0009\Gamma$ with $g = 2.25$ and a voltage bias of $V = 0.03\Gamma$ after the dot level has been switched to its final position.

Fourier transform of the retarded Green's function, sidebands start getting drastically smaller away from the main Kondo peak, resulting in less interference with it. Therefore, the oscillation amplitude associated with these peaks is negligible compared to the one associated with the first sideband, leading to the absence of other frequencies.

Before we conclude, we would like to address the effect of finite bias on the above reported time-dependent conductance. It is well known that the bias would split the main elastic Kondo peak into two parts, each of which are pinned to the Fermi level of the contacts. These split Kondo resonances would induce split Kondo peak oscillations in the transient current with a frequency equal to the bias V in the absence of any electron–phonon coupling [19]. Therefore, the effect of the bias on the above system is twofold. First, the steady state conductance would be lower than for the infinitesimal bias case since the Kondo effect is gradually destroyed with the bias. In fact, steady state investigations of a system with strong electron–electron and electron–phonon interaction in a finite bias showed that the differential conductance exhibits enhancements when the bias is an integer multiple of the phonon frequency ω_0 [43]. This is due to the fact that the inelastic phonon sidebands overlap with the split Kondo peaks. Indeed, this behavior is reminiscent of the time averaged conductance of an ac driven quantum dot [54].

In the time-dependent case, there are two interference effects taking place simultaneously, namely between the split main Kondo peaks and between each split main Kondo peak and its phonon sidebands. Obviously, this results in two distinct oscillation frequencies. This beating gives rise to more complicated oscillations in the transient current, as seen in figure 6. When we take the Fourier transform of the transient current, we are able to identify these two distinct frequencies corresponding to the bias V and the phonon frequency ω_0. This result unambiguously confirms the validity of the above interpretation. When the bias is equal to ω_0, the behavior of the transient current is similar to that in the zero-bias case even though the dot density of states is entirely different. In this case, only one oscillation frequency survives and it is equal to ω_0 because the two interference processes are in resonance.

4. Conclusions

In conclusion, the non-crossing approximation was utilized in this paper to investigate the combined effect of strong electron–electron and electron–phonon interaction on the instantaneous conductance in a single-molecule transistor when the dot level is suddenly shifted to a position where the Kondo resonance is present. Our results clearly showed that the instantaneous conductance displays decaying sinusoidal oscillations on the long timescale in an infinitesimal bias. This fact sets these novel oscillations apart from the previously predicted split Kondo peak oscillations [19].

Investigation of the amplitude of these oscillations indicated that it sensitively depends on the ambient temperature and the electron–phonon coupling strength. Moreover, the frequency of these oscillations was found to be precisely equal to the phonon frequency upon taking the Fourier transform of the instantaneous conductance on the long timescale. On the basis of these observations and investigation of the density of states of the quantum dot, we proposed that the origin of this novel phenomenon can be attributed as the interference between the main elastic Kondo peak and its phonon sidebands. We also uncovered that finite source–drain bias results in more complicated transient oscillations in the instantaneous conductance. Two distinct frequencies corresponding to the phonon frequency ω_0 and bias voltage V play a role in this case.

We believe that the phenomenon discussed in this paper could be observed with present day ultrafast transient experimental techniques [55] since it takes place on the longest timescale which is typically of the order of tens of picoseconds. Also, the theory presented here depicts a fairly realistic assessment of the single-molecule junctions as it takes into account both Coulomb and vibrational interactions that are ubiquitous for real molecules. Thus we hope to invigorate this field by motivating a new experiment with the predictions made in this paper.

References

[1] Aviram A and Ratner M A 1974 *Chem. Phys. Lett.* **29** 277
[2] Kroto H W, Heath J R, O'Brien S C, Curl S C and Smalley R E 1985 *Nature* **318** 162
[3] Ng T K and Lee P A 1988 *Phys. Rev. Lett.* **61** 1768
[4] Glazman L I and Raikh M E 1988 *JETP Lett.* **47** 452
[5] Goldhaber-Gordon D, Shtrikman H, Mahalu D, Abusch-Magder D, Meirav U and Kastner M A 1998 *Nature* **391** 156–9
[6] Goldhaber-Gordon D, Gores J, Kastner M A, Shtrikman H, Mahalu D and Meirav U 1998 *Phys. Rev. Lett.* **81** 5225–8
[7] Cronenwett S M, Osterkamp T H and Kouwenhoven L P 1998 *Science* **281** 540–4
[8] Park J *et al* 2002 *Nature* **417** 722
[9] Liang W J, Shores M P, Bockrath M, Long J R and Park H 2002 *Nature* **417** 725
[10] Rocha A R, Garcia-Suarez V M, Bailey S W, Lambert C J, Ferrer J and Sanvito S 2005 *Nat. Mater.* **4** 335
[11] Seneor P, Bernand-Mantel A and Petroff F 2007 *J. Phys.: Condens. Matter* **19** 165222
[12] Kondo J 1964 *Prog. Theor. Phys.* **32** 37
[13] Hewson A C 1993 *The Kondo Problem to Heavy Fermions* (Cambridge: Cambridge University Press)
[14] Ashoori R C 1996 *Nature* **379** 413
[15] Nordlander P, Pustilnik M, Meir Y, Wingreen N S and Langreth D C 1999 *Phys. Rev. Lett.* **83** 808–11
[16] Plihal M, Langreth D C and Nordlander P 2000 *Phys. Rev.* B **61** R13341–4
[17] Schiller A and Herschfield S 2000 *Phys. Rev.* B **62** R16271–4
[18] Merino J and Marston J B 2004 *Phys. Rev.* B **69** 115304
[19] Plihal M, Langreth D C and Nordlander P 2005 *Phys. Rev.* B **71** 165321
[20] Anders F B and Schiller A 2005 *Phys. Rev. Lett.* **95** 196801
[21] Anders F B and Schiller A 2006 *Phys. Rev.* B **74** 245113
[22] Izmaylov A F, Goker A, Friedman B A and Nordlander P 2006 *J. Phys.: Condens. Matter* **18** 8995–9006
[23] Goker A, Friedman B A and Nordlander P 2007 *J. Phys.: Condens. Matter* **19** 376206
[24] Goker A, Zhu Z Y, Manchon A and Schwingenschlogl U 2010 *Phys. Rev.* B **82** 161304(R)
[25] Gull E, Werner P, Parcollet O and Troyer M 2008 *Europhys. Lett.* **82** 57003
[26] Werner P, Oka T and Millis A J 2009 *Phys. Rev.* B **79** 035320
[27] Schmidt T L, Werner P, Muhlbacher L and Komnik A 2008 *Phys. Rev.* B **78** 235110
[28] Galperin M, Ratner M A and Nitzan A 2007 *J. Phys.: Condens. Matter* **19** 103201
[29] Stipe B C, Rezaei M A and Ho W 1999 *Phys. Rev. Lett.* **82** 1724
[30] Hahn J R, Lee H J and Ho W 2000 *Phys. Rev. Lett.* **85** 1914
[31] Migdal A B 1958 *Sov. Phys.—JETP* **7** 996
[32] Eliashberg G M 1960 *Sov. Phys.—JETP* **11** 696
[33] Frederiksen T, Brandbyge M, Lorente N and Jauho A P 2004 *Phys. Rev. Lett.* **93** 256601
[34] Mii T, Tikhodeev S G and Ueba H 2003 *Phys. Rev.* B **68** 205406
[35] Galperin M, Ratner M A and Nitzan A 2004 *Nano Lett.* **4** 1605
[36] Galperin M, Ratner M A and Nitzan A 2004 *J. Chem. Phys.* **121** 11965
[37] Yu L H and Natelson D 2004 *Nano Lett.* **4** 79
[38] Zhu J X and Balatsky A V 2003 *Phys. Rev.* B **67** 165326
[39] Lundin U and McKenzie R H 2002 *Phys. Rev.* B **66** 075303
[40] Chen Z Z, Lu R and Zhu B F 2005 *Phys. Rev.* B **71** 165324
[41] Galperin M, Nitzan A and Ratner M A 2006 *Phys. Rev.* B **73** 045314
[42] Wang R Q, Zhou Y Q, Wang B and Xing D Y 2007 *Phys. Rev.* B **75** 045318
[43] Paaske J and Flensberg K 2005 *Phys. Rev. Lett.* **94** 176801
[44] Yong H-C, Yang K-H and Tian G-S 2007 *Commun. Theor. Phys.* **48** 1107
[45] Galperin M, Nitzan A and Ratner M A 2007 *Phys. Rev.* B **76** 035301
[46] Riwar R P and Schmidt T L 2009 *Phys. Rev.* B **80** 125109
[47] Lang I G and Firsov Y A 1963 *Sov. Phys.—JETP* **16** 1301
[48] Jauho A P, Wingreen N S and Meir Y 1994 *Phys. Rev.* B **50** 5528
[49] Werner P and Millis A J 2007 *Phys. Rev. Lett.* **99** 146404
[50] Shao H X, Langreth D C and Nordlander P 1994 *Phys. Rev.* B **49** 13929–13947
[51] Yang K H, Zhao Y L, Wu Y J and Wu Y P 2010 *Phys. Lett.* A **374** 2874
[52] Muhlbacher L and Rabani E 2008 *Phys. Rev. Lett.* **100** 176403
[53] Yang K H, Wu Y P and Zhao Y L 2010 *Europhys. Lett.* **89** 37008
[54] Goker A 2008 *Solid State Commun.* **148** 230
[55] Terada Y, Yoshida S, Takeuchi O and Shigekawa H 2010 *J. Phys.: Condens. Matter* **22** 264008